INTERNATIONAL JOURNAL FOR NUMERICAL METHODS IN FLUIDS
Int. J. Numer. Meth. Fluids 2002; **39**:1139–1159 (DOI: 10.1002/fld.355)

On the validity of the perturbation approach for the flow inside weakly modulated channels

H. Zhou, R. E. Khayat*,†, R. J. Martinuzzi and A. G. Straatman

Department of Mechanical and Materials Engineering, The University of Western Ontario, London, Ontario, Canada N6A 5B9

SUMMARY

The equations governing the flow of a viscous fluid in a two-dimensional channel with weakly modulated walls have been solved using a perturbation approach, coupled to a variable-step finite-difference scheme. The solution is assumed to be a superposition of a mean and perturbed field. The perturbation results were compared to similar results from a classical finite-volume approach to quantify the error. The influence of the wall geometry and flow Reynolds number have extensively been investigated. It was found that an explicit relation exists between the critical Reynolds number, at which the wall flow separates, and the dimensionless amplitude and wavelength of the wall modulation. Comparison of the flow shows that the perturbation method requires much less computational effort without sacrificing accuracy. The differences in predicted flow is kept well around the order of the square of the dimensionless amplitude, the order to which the regular perturbation expansion of the flow variables is carried out. Copyright © 2002 John Wiley & Sons, Ltd.

1. INTRODUCTION

Viscous flow in a micro-channel with modulated walls is a classical problem that has attracted renewed interest because of its immediate relevance to novel micro-technologies, for example, compact heat exchangers with high heat flux or membrane blood oxygenators in extra-corporeal systems [1]. In spite of the apparent geometrical simplicity, these flows can contain separated flow regions and exhibit many of the features present in much more complex geometries, which can significantly impact heat or mass transfer performance. This richness in physical phenomena in a relatively simple geometry motivates fundamental interest by providing an ideal setting for developing and testing the accuracy and efficacy of numerical procedures to solve of the Navier–Stokes equations.

Stephanoff *et al.* [2] were among the first to experimentally investigate the two-dimensional steady, unsteady, and oscillatory flow in a furrowed channel at low Reynolds numbers for a

* Correspondence to: R. E. Khayat, Department of Mechanical and Materials Engineering, The University of Western Ontario, London, Ontario, Canada N6A 5B9.
† E-mail: rkhayat@eng.uwo.ca

Contract/grant sponsor: Natural Sciences and Engineering Council of Canada

Received August 2001
Revised November 2001

modelled Oxford membrane blood oxygenator. Their work provided some qualitative support for the numerical model proposed by Sobey [1], based on a streamline–vorticity formulation. A further contribution to the flow characteristics in modulated channels was given by Nishimura *et al.* [3], who performed measurements in the Reynolds number range 40–10 000 to observe the steady flow characteristics in a channel with symmetric wavy walls and provided an empirical relationship between wall shear stress and flow Reynolds number. Later, Nishimura *et al.* [4] performed another experimental investigation focusing on mass transfer from a channel with symmetric sinusoidal walls or arc-shaped walls.

Several numerical studies exist for the prediction of low-Reynolds-number flow in wavy channels. These can be broadly categorized as those dealing with heat/mass transfer characteristics, which necessarily focus on a narrow range of geometrical parameters [4–7], or on hydrodynamic simulations [1–3, 8–12]. These studies have focused on the steady-state behaviour. The unsteady non-isothermal flow was considered by Wang and Vanka [13]. Of the latter, much effort has been dedicated to developing solution techniques or suitable formulations for the problem. The techniques either consist of solving the Navier–Stokes equations or solving a perturbation problem either in terms of primitive or streamline–vorticity variables. The advantage of the perturbation approach is that it can be much faster than a full simulation, but, due to the truncation inherent in the method, is subject to larger uncertainties. There is, however, little literature dedicated to quantification of the accuracy or comparison of different techniques.

The existing numerical techniques can be divided into three categories depending on the formulation of the physical domain. In a first approach, the modulated flow domain is mapped onto a rectangular computational domain to simplify the boundary conditions and to facilitate the integration process [14]. Benjamin [8] considered a co-ordinate system based on streamlines of inviscid flow over a wavy wall in his analysis of shear flow over wavy walls. Sobey [1] analysed the flow through furrowed channels and used an analytical mapping resulting in a non-orthogonal co-ordinate system. Caponi *et al.* [15] employed an orthogonal transformation expressed in terms of an infinite Fourier series in their analysis of boundary layers over modulated surfaces. Tanda and Vittori [5] carried out the investigation of fluid flow and heat transfer in a two-dimensional wavy channel by using another non-orthogonal transformation [6].

In a second approach, the problem is solved directly in the physical domain such that the governing equations retain a very simple form. However, one has to develop special procedures for the imposition of boundary conditions. The most popular procedure is following a perturbation method, which involves the transfer of boundary conditions to a certain mean location of the boundary, resulting in a regular computational domain [9]. The accuracy of this approach depends on the amplitude of the modulation and the type of boundary conditions transfer procedure. This method is of interest due to its simplicity and due to the fact that in many applications, the interest lies in small modulation where the perturbation method provides reasonable accuracy. Vajaravelu and Kharagpur [7] applied this perturbation method, carrying out a numerical study of flow through weakly modulated wavy channels. Selvarajan *et al.* [10] adopted the same method studying stability characteristics of wavy walled channel flow. An accurate spectral approach has also been implemented by Deane *et al.* [16] to simulate the flow inside converging–diverging channels. Szumbarski and Floryan [17] also developed a direct spectral method for the determination of flows over corrugated boundaries. They, however, treat the flow problem as an internal rather than a boundary-value problem, where the flow conditions are specified along a line in the interior of a computational domain.

A third approach is the combination of the above two approaches. By taking advantage of the mapping approach, one also adopts the essence of the perturbation method to reduce the complicated transformed governing equations into a set of ordinary differential equations subject to simple boundary conditions. Tsangaris and Leiter [11] performed a study on laminar steady flow in sinusoidal channels by this method. Selvarajan *et al.* [12] also employed this method to investigate the flow through wavy- walled channels. As stated before, the accuracy of this approach depends on the amplitude of the modulation.

Finally, it is also worth mentioning some of the studies conducted on unsteady flow. Guzman and Amon [18, 19] carried out a direct three-dimensional numerical simulation in a fully developed periodic regime for a uniform heat flux density at the bottom wall; the top wall was assumed to be adiabatic. Beyond a critical Reynolds number, they showed the existence of an unsteady periodic behaviour with higher harmonics. As the Reynolds number is increased further, a quasi-periodic behaviour is observed, with two incommensurable frequencies (torus T2). The flow eventually exhibits chaotic behaviour. The onset of unsteady motion is in accord with the linear stability analysis of Blancher *et al.* [20].

The present paper aims to correct two apparent deficiencies gleaned from the above literature review. First, there has not been a systematic investigation of the uncertainty of results obtained with the perturbation method. Second, the influence of the channel modulation amplitude, ε, and wavelength, λ, on the critical Reynolds number for the appearance flow reversal has been studied only over a very small range. Thus, in the first part of the paper, the error resulting from a perturbation analysis is investigated in terms of ε and the wall wave number, $\alpha = 2\pi/\lambda$. Since results for experiments with $\varepsilon < 0.3$ still do not find a consensus [11], results will be benchmarked against results obtained from a traditional finite-volume formulation. The hydrodynamic features of steady flow in modulated channels will then be described in a systematic and coherent way. In the following section, the problem formulation and solution procedure are described. The third section introduces the numerical assessment. In the fourth section, the present findings, expressed in terms of Reynolds number, dimensionless amplitude and wall wave number are discussed. Some conclusions are drawn in the last section.

2. PROBLEM FORMULATION AND SOLUTION PROCEDURE

In this section, the general equations and boundary conditions for the Poiseuille flow with spatially modulated walls are derived for small-amplitude modulation. A regular perturbation expansion for the flow field is carried out after the equations are mapped over a rectangular domain, reducing the problem to a set of ordinary differential equations, which will be solved using a variable-step-finite-difference scheme.

2.1. Governing equations

Consider the steady-state flow of an incompressible Newtonian fluid of constant density ρ and viscosity μ. The fluid is assumed to lie between two infinite rigid boundaries, the lower being straight and the upper being periodically modulated. The problem is first introduced in the (X, Y) plane, with the X-axis being located along the lower wall. The general shapes of the lower and upper walls are given by $Y = 0$ and $D + Af(X)$, respectively, where A is the modulation amplitude, and D is the mean gap width. Here $f(X)$ is a general function of X

that may be arbitrarily prescribe. In this work, however, only a sinusoidal modulation will be considered.

The general conservation of mass and linear momentum equations are given by

$$\nabla \cdot \mathbf{U} = 0 \tag{1a}$$

$$\rho \mathbf{U} \cdot \nabla \mathbf{U} = \mu \nabla^2 \mathbf{U} - \nabla P \tag{1b}$$

where $\mathbf{U}(U, V)$ is the velocity vector, P is the pressure and ∇ is the gradient operator. The fluid is assumed to adhere to the rigid walls, and the no-slip boundary conditions are written as

$$U(X, Y = 0) = U(X, Y = D + Af) = 0 \tag{2}$$

The dimensionless co-ordinates, x and y, velocity components u and v and the pressure p, are introduced as follows:

$$x = \frac{X}{D}, \quad y = \frac{Y}{D}, \quad u = \frac{U}{U_{\max}}, \quad v = \frac{V}{U_{\max}}, \quad p = \frac{DP}{\mu U_{\max}} \tag{3}$$

where $U_{\max}$ is the maximum velocity corresponding to an equivalent linear pressure gradient imposed on the Poiseuille flow between two flat plates coinciding with the mean heights of the modulated walls. After the dimensionless variables are introduced, two dimensionless groups emerge in the problem, namely, the Reynolds number and the aspect ratio ε:

$$Re = \frac{\rho U_{\max} D}{\mu}, \qquad \varepsilon = \frac{A}{D} \tag{4}$$

The governing equations become

$$u_x + v_y = 0 \tag{5a}$$

$$Re(uu_x + vu_y) = u_{xx} + u_{yy} - p_x \tag{5b}$$

$$Re(uv_x + vv_y) = v_{xx} + v_{yy} - p_y \tag{5c}$$

where a subscript denotes partial differentiation. The above equations must be solved subject to the no-slip condition

$$u(x, y = 0) = u(x, y = 1 + \varepsilon f(x)) = v(x, y = 0) = v(x, y = 1 + \varepsilon f(x)) = 0 \tag{6a}$$

It is further assumed that the flow field (velocity and pressure) is spatially periodic, commensurately with the wall modulation. This periodicity condition is written as

$$\begin{aligned} u(x = 0, y) &= u(x = 2\pi/\alpha, y) \\ v(x = 0, y) &= v(x = 2\pi/\alpha, y) \\ p(x = 0, y) &= p(x = 2\pi/\alpha, y) \end{aligned} \tag{6b}$$

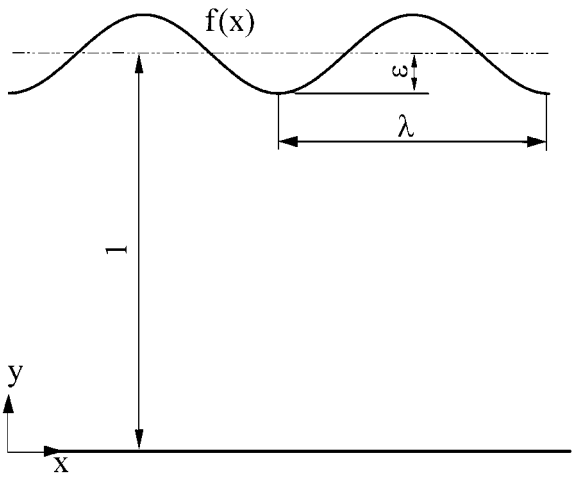

Figure 1. Physical domain and flow configuration for spatially modulated channel.

where α is the dimensionless wave number of the wall modulation. The problem (5)–(6) is defined over the physical domain $\Omega_{xy} = \{(x, y) \mid x \in [0, 2\pi/\alpha], y \in [0, 1 + \varepsilon f(x)]\}$, which is next mapped onto the rectangular domain. The physical domain and flow configuration are schematically illustrated in Figure 1.

2.2. *Domain transformation*

The periodic physical domain Ω_{xy} is mapped onto the rectangular domain $\Omega_{\xi\eta} = \{(\xi, \eta) \mid \xi \in [0, 2\pi/\alpha], \eta \in [0, 1]\}$. In this case

$$\xi(x, y) = x, \qquad \eta(x, y) = \frac{y}{h(x)} \tag{7}$$

where $h(x) = 1 + \varepsilon f(x)$ is the dimensionless gap. Now the transformed equations read,

$$u_\xi - \frac{\eta h'}{h} u_\eta + \frac{1}{h} v_\eta = 0 \tag{8a}$$

$$\begin{aligned} Re \left[u \left(u_\xi - \frac{\eta h'}{h} u_\eta \right) + \frac{v u_\eta}{h} \right] = & - p_\xi + \frac{\eta h'}{h} p_\eta + \frac{u_{\eta\eta}}{h^2} \\ & + u_{\xi\xi} - \eta \left[\left(\frac{h''}{h} - \left(\frac{h'}{h} \right)^2 \right) u_\eta + \frac{h'}{h} u_{\eta\xi} \right] \\ & - \frac{\eta h'}{h} \left(u_{\xi\eta} - \frac{\eta h'}{h} u_{\eta\eta} - \frac{h'}{h} u_\eta \right) \end{aligned} \tag{8b}$$

$$Re\left[u\left(v_\xi - \frac{\eta h'}{h}\, v_\eta\right) + \frac{v v_\eta}{h}\right] = \frac{-p_\eta}{h} + \frac{v_{\eta\eta}}{h^2} + v_{\xi\xi} - \eta\left[\left(\frac{h''}{h} - \left(\frac{h'}{h}\right)^2\right) v_\eta + \frac{h'}{h}\, v_{\eta\xi}\right] - \frac{\eta h'}{h}\left(v_{\xi\eta} - \frac{\eta h'}{h}\, v_{\eta\eta} - \frac{h'}{h}\, v_\eta\right) \tag{8c}$$

where a prime denotes total differentiation. The boundary conditions are

$$u(\xi, \eta = 0) = u(\xi, \eta = 1) = v(\xi, \eta = 0) = v(\xi, \eta = 1) = 0 \tag{9a}$$

$$u(\xi = 0, \eta) = u(\xi = 2\pi/\alpha, \eta)$$

$$v(\xi = 0, \eta) = v(\xi = 2\pi/\alpha, \eta) \tag{9b}$$

$$p(\xi = 0, \eta) = p(\xi = 2\pi/\alpha, \eta)$$

The solution to Equations (8) is sought subject to conditions (9). This is a difficult non-linear two-dimensional problem, with variable coefficients in the governing equations. There are, however, some limit flows that may be considered, which can simultaneously be of practical and fundamental significance.

2.3. The perturbation expansion

In this work, only small-amplitude modulation is examined, so that ε is small ($\varepsilon \ll 1$). A regular perturbation expansion is used on the velocity and pressure:

$$u = u^0 + \varepsilon u^1 + O(\varepsilon^2), \quad v = v^0 + \varepsilon v^1 + O(\varepsilon^2), \quad p = p^0 + \varepsilon p^1 + O(\varepsilon^2) \tag{10}$$

where terms of $O(\varepsilon^2)$ and higher are neglected. Substitution of expressions (10) into Equations (8) and conditions (9) leads to a hierarchy of equations and boundary conditions that must be solved to each order in ε. Thus, to leading order in ε, one recovers the equations encountered in conventional Poiseuille flow. Correspondingly, the solution is given by

$$u^0 = 4\eta(1 - \eta), \quad v^0 = 0, \quad p^0_\xi = -8 \tag{11}$$

The equations to $O(\varepsilon)$ become

$$u^1_\xi + v^1_\eta = u^0_\eta \eta f' \tag{12a}$$

$$Re(u^0 u^1_\xi - u^0 \eta f' u^1_\eta + u^0_\eta v^1) + p^1_\xi - u^1_{\xi\xi} - u^1_{\eta\eta} = -2u^0_{\eta\eta} f - u^0_\eta \eta f'' \tag{12b}$$

$$Re\, u^0 v^1_\xi + p^1_\eta - v^1_{\xi\xi} - v^1_{\eta\eta} = 0 \tag{12c}$$

which must be solved subject to

$$u^1(\xi,\eta=0)=u^1(\xi,\eta=1)=v^1(\xi,\eta=0)=v^1(\xi,\eta=1)=0 \tag{13a}$$

$$\begin{aligned} u^1(\xi=0,\eta)&=u^1(\xi=2\pi/\alpha,\eta)\\ v^1(\xi=0,\eta)&=v^1(\xi=2\pi/\alpha,\eta)\\ p^1(\xi=0,\eta)&=p^1(\xi=2\pi/\alpha,\eta) \end{aligned} \tag{13b}$$

Note that the second expression in (11) has been used.

2.4. Solution procedure

At this point, it is necessary to introduce explicitly the modulated wall profile f. Various configurations may be easily incorporated in the general formulation above. For instance, both walls could be assumed to be modulated, and the modulation can be represented by a general Fourier series, as long as it is smooth. In this work, however, only the upper wall is assumed to be modulated in the form of a sine wave such that

$$f(\xi)=\sin(\alpha\xi) \tag{14}$$

where α is the (dimensionless) wavenumber. In this case, the general solution of Equations (12) is given as

$$\begin{aligned} u^1(\xi,\eta) &= u^{11}(\eta)\sin(\alpha\xi)+u^{12}(\eta)\cos(\alpha\xi)\\ v^1(\xi,\eta) &= v^{11}(\eta)\sin(\alpha\xi)+v^{12}(\eta)\cos(\alpha\xi)\\ p^1(\xi,\eta) &= p^{11}(\eta)\sin(\alpha\xi)+p^{12}(\eta)\cos(\alpha\xi) \end{aligned} \tag{15}$$

where $u^{11}, u^{12}, v^{11}, v^{12}, p^{11}$ and p^{12} are unknown coefficients. It is important to observe that, it is the linear nature of Equations (12) that allows the solution to be expressed as in (15), which may then be regarded as the most general solution. If, for instance, the wall assumes other forms than sinusoidal, then additional modes must be included. Substituting the above expressions into Equations (12), the governing equations for the coefficients become

$$\begin{aligned} u^{11}\alpha+v^{12}_{\eta} &= \alpha u^0_{\eta}\eta\\ -u^{12}\alpha+v^{11}_{\eta} &= 0\\ p^{11}\alpha+Re(u^0u^{11}\alpha+u^0_{\eta}v^{12}-\alpha u^0u^0_{\eta}\eta)+\alpha^2u^{12}-u^{12}_{\eta\eta} &= 0\\ -p^{12}\alpha+Re(-u^0u^{12}\alpha+u^0_{\eta}v^{11}-\alpha^2u^0_{\eta}\eta+2u^0_{\eta\eta})+\alpha^2u^{11}-u^{11}_{\eta\eta} &= 0\\ p^{12}_{\eta}\alpha+Re\,u^0v^{11}\alpha+\alpha^2v^{12}-v^{12}_{\eta\eta} &= 0\\ p^{11}_{\eta}\alpha-Re\,u^0v^{12}\alpha+\alpha^2v^{11}-v^{11}_{\eta\eta} &= 0 \end{aligned} \tag{16}$$

The system above is a set of non-homogeneous ordinary differential equations, which together with the corresponding homogeneous boundary conditions

$$u^{11}=u^{12}=v^{11}=v^{12}=0 \quad \text{at } \eta=0 \text{ and } \eta=1 \tag{17}$$

constitute a boundary-value problem of the two-point type. It is solved using a variable-step finite-difference scheme (IMSL-DBVPFD). The basic discretization is the trapezoidal rule over a non-uniform mesh. This mesh is chosen adaptively, to make the local error approximately the same size everywhere. Higher-order discretizations are obtained by differed corrections and global error estimates are produced to control the computation. The linear system of equations is solved using a special form of Gauss elimination that preserves sparseness.

3. NUMERICAL ASSESSMENT

A review of the literature shows that the limitations and advantages of perturbation methods in predicting flows in weakly modulated channels have not been rigorously investigated. Since the present method is intended to provide a fast and accurate alternative to conventional CFD calculations in the limit of small modulation amplitudes, establishing the accuracy of the solution is critical. In this section, a detailed study of the influence of geometric parameters and Reynolds number on solution accuracy and a comparison to finite-volume predictions is provided.

Error sources are in the truncated terms of the governing equations. These terms contain combinations of the velocity gradients multiplied by coefficients containing the parameters α, ε and Re. Assuming that the (dimensionless) velocity gradients are of order 1, the error in the perturbation method should scale with the higher-order coefficients of order ε^2 and $\alpha\varepsilon^2$. The influence of the truncated terms on the continuity equation is conveniently summarized through the global error in mass conservation, since only the mean pressure gradient is imposed in the solution procedure. In general, mass is not conserved, and the volume flow rate, $Q(x)$, varies (locally) with x. This variation is typically illustrated in Figure 2, where the streamwise dependence of the predicted volume flow rate is shown for several values of $\varepsilon, \alpha = 1$ and

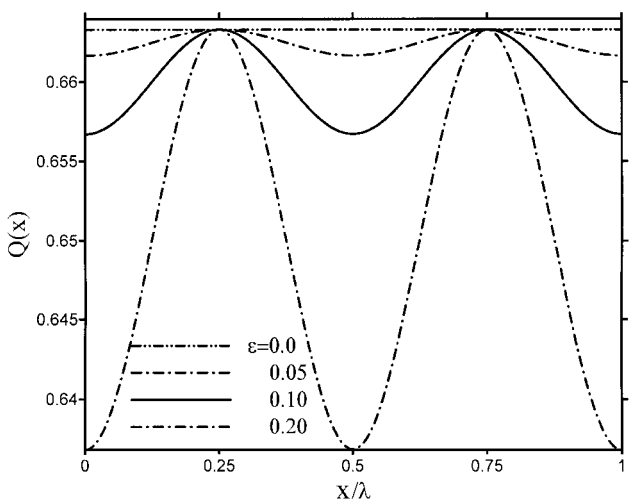

Figure 2. Streamwise variation of the predicted volume flow rate for $Re = 3000$ and $\alpha = 1.0$.

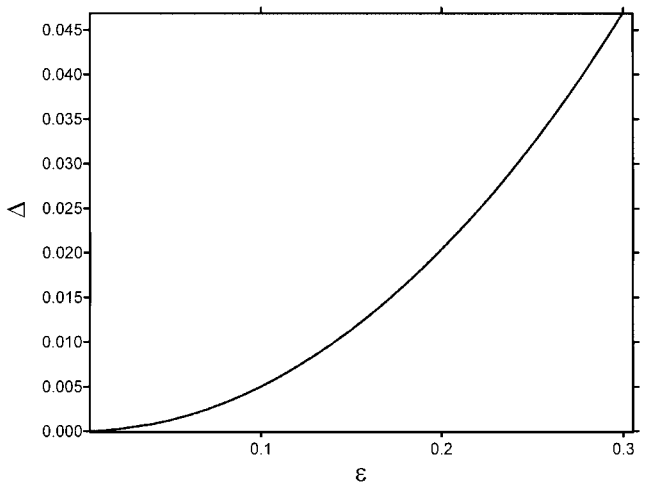

Figure 3. Maximum error for mass conservation, Δ, as a function of the wall modulation, ε. Calculations show that the influence of the modulation wavenumber and inertia on the error is essentially absent. The curve in the figure is essentially universal.

$Re = 3000$. The fluctuation in $Q(x)$ is in phase with the wall modulation, and this fluctuation increases with modulation amplitude, ε. The maximum in Q, however, remains the same, corresponding to Poiseuille flow ($Q = \frac{2}{3}$). The flow rate that is averaged over a modulation wavelength, Q_{ave}, is then considered as the exact value for Q, and the difference $Q - Q_{\text{ave}}$ is then taken as a measure of inaccuracy. This average decreases with ε. The figure indicates that the maximum error occurs at the crests and troughs of the modulation wave of the wall, and is zero at the inflection points, where $y = 1$, which is expected since the truncated terms are multiplied by the sinusoidal waveform. The global error at a given streamwise location may then be defined as

$$\Delta = \frac{|Q - Q_{\text{ave}}|_{\max}}{Q_{\text{ave}}} \tag{18}$$

The influence of ε on the maximum error is shown in Figure 3. The influence of the wavenumber of the wall modulation and inertia on the overall error is negligible. This observation is based on calculations for the ranges $0.1 < \alpha < 100$ and $50 < Re < 5000$. It is expected that these two parameters contribute little to Δ since truncation with respect to ε only is imposed. As expected, the error behaves like ε^2 and conservation of mass is satisfied to within 1% for $\varepsilon < 0.15$.

A more rigorous validation of the perturbation solution follows from direct comparison with simulation results obtained using a CFD code based on the finite-volume discretization procedure [21]. The finite-volume code developed by El-Soukkary includes special periodic boundary conditions that allow for the imposition of a mass flow rate, which makes the computation more straightforward when a specific flow Re is desired. Thus, for the present computations, periodic conditions were imposed at the inlet and outlet, with the additional constraint of a mass flow rate. No-slip and zero-penetration conditions were imposed on the

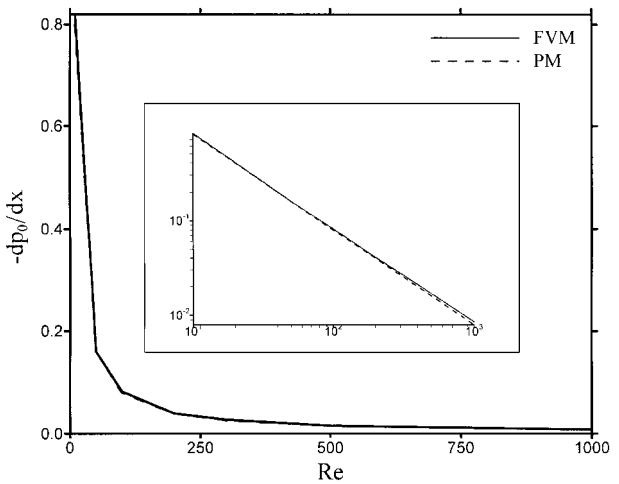

Figure 4. Comparison of the variation of the (linear) pressure gradient with Reynolds number for $\varepsilon = 0.1$ and $\alpha = 1.0$. Inset shows the log–log plot.

upper and lower walls. To ensure that the finite-volume predictions were independent of the spatial step size, a grid-independence study was carried out for the case of $\alpha = 1$, $\varepsilon = 0.1$ and $Re = 3000$ (the highest Reynolds number considered in this study). The grid density was progressively doubled until the results were grid-converged to within 1%; results presented in this study were computed on grids of 160×100 cells.

For comparison between the perturbation and finite-volume methods, the driving (linear) pressure is first imposed, and the perturbation solution yields a mass flow rate, which, in turn is used in the CFD code to generate the flow field. Simultaneously, a linear driving pressure is also generated by the code, which is compared against the original imposed pressure used for the perturbation method. The comparison is typically illustrated in Figure 4, which clearly shows close agreement between the two methods. The pressure gradient is plotted against Re for $\varepsilon = 0.1$ and $\alpha = 1$. The log–log plot indicates, upon amplification, more clearly the level of discrepancy between the two methods. The relative error is usually found to be on the order of a few per cent.

The mean flow patterns obtained using the two methods are very similar as seen, for example, from the streamline plots of Figure 5 for $Re = 3000$, $\varepsilon = 0.1$ and $\alpha = 1$. The streamlines are defined as iso-contours of the streamfunction obtained by integrating the streamwise velocity component from the lower wall. To maintain consistency in the streamfunction definition between adjacent streamwise locations, the small error of order ε^2 on the mass flow is corrected by normalizing the entire profile by the local mass flow. The resulting streamline patterns are qualitatively indistinguishable from those of the finite-volume simulation.

Quantitatively, the more sensitive parameters are the critical Reynolds number for separation, the location of the separation and reattachment points. Typical predictions using both methods are summarized in Table I. Differences in the prediction of the separation point differ by less than 1% and are thus of order ε^2. However, differences in the predictions of the reattachment point are much larger, of the order of 5% (order ε) and increase as Re

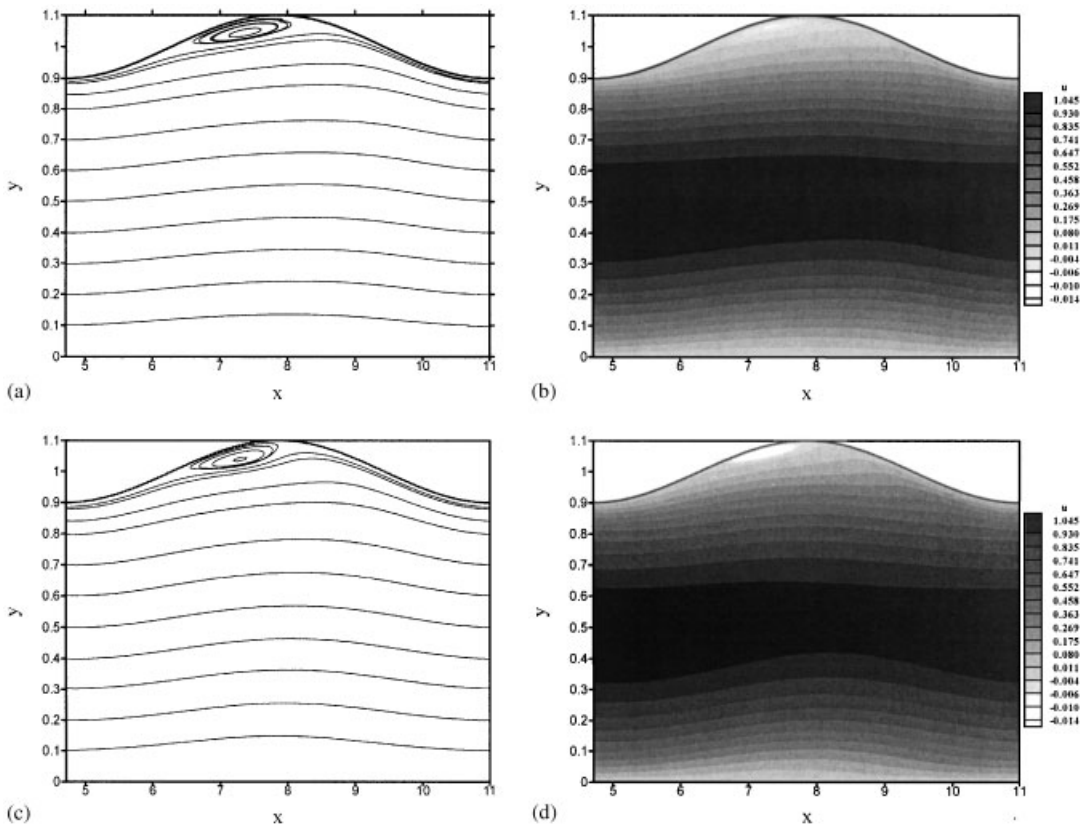

Figure 5. Comparison of mean flow patterns and u-contours based on the finite-volume (a, b) and the perturbation (c, d) methods for $Re = 3000$, $\varepsilon = 0.1$ and $\alpha = 1$.

Table I. Variation in separation and reattachment points with Reynolds number ($\varepsilon = 0.1$, $\alpha = 1.0$).

Re	FVM separation point	PM separation point	Error (%)	FVM reattachment point	PM reattachment point	Error (%)
2500	6.527	6.503	0.37	8.133	7.885	3.05
3000	6.387	6.377	0.16	8.377	7.948	5.12
3500	6.283	6.314	0.50	8.482	8.011	5.56

increases. The corresponding u-contours are also shown in Figure 5, which also reflect close agreement. However, a better quantitative assessment is obtained by comparing the streamwise velocity profiles based on the finite-volume and perturbation simulations at a given location. This comparison is shown in Figure 6 for $Re = 3000$ and $\varepsilon = 0.1$. The locations, $x = \lambda/2$ and λ, coincide, respectively, with a crest and a trough, where the error is greatest. The figure shows the y-distribution of the total streamwise velocity component, u, and the

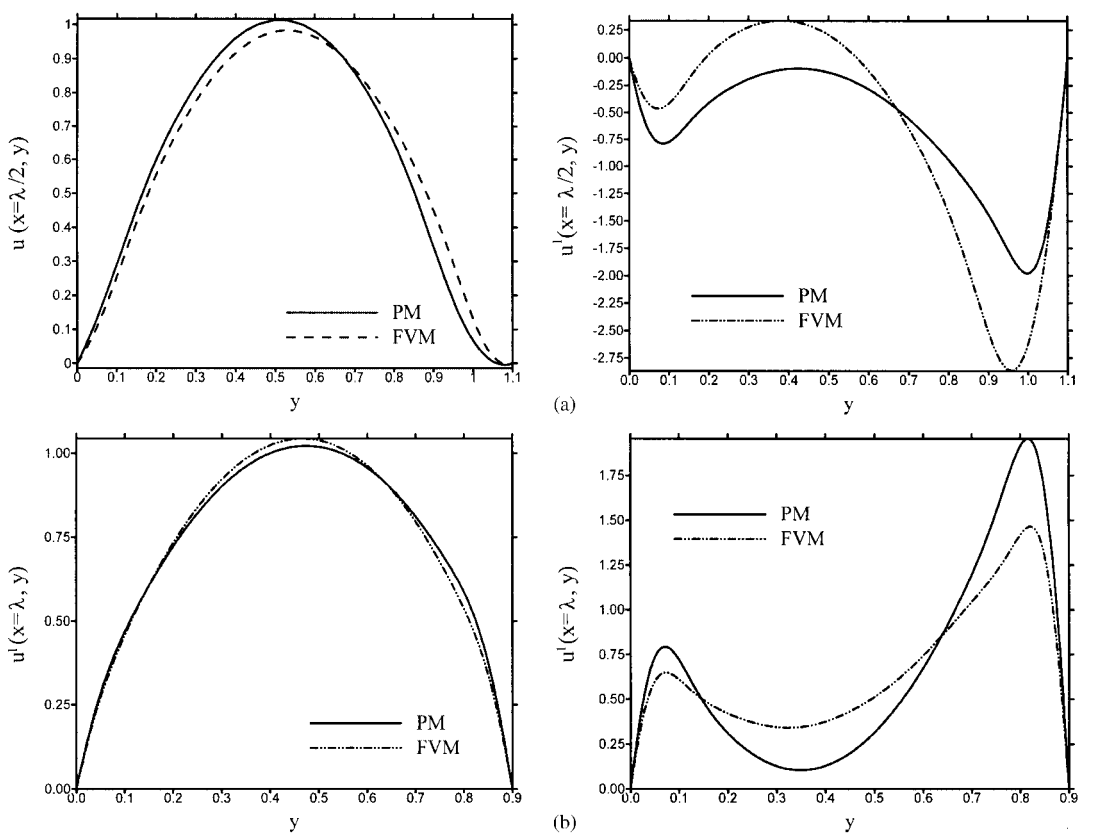

Figure 6. Streamwise velocity distribution (a) below the crest at $x = \lambda/2$, and (b) below the trough at $x = \lambda$, for $Re = 3000$, $\varepsilon = 0.1$ and $\alpha = 1$. The figure shows the distributions based on the finite-volume and perturbation methods.

perturbation contribution, u^1. The perturbation component differs from the CFD simulation results by an order ε. The overall solution is consequently accurate to within ε^2. It is noteworthy that the trend in u^1 is correctly predicted at all points and the error is in the magnitude. In other words, the location of the critical points in the profile, specifically zero stress, extrema and inflection points, are all correctly predicted. As a result, the predicted critical Reynolds number, i.e. when flow separation first appears, by both methods coincides. The predicted streamwise pressure evolution is shown in Figure 7 for $\varepsilon = 0.1$ and $\alpha = 1$. The pressure at each streamwise location is computed as an area-weighted pressure, and thus corresponds to that pressure required to exert an equivalent force at that location. The difference in prediction between the finite-volume and perturbation results is of the order of ε, approximately 5%, and is typical for all tests conducted. These results are consistent with the general formulation. By inspection, the leading truncation term for u^1 is of order ε, cf. Equation (12a) and thus, from Equation (12b), the pressure gradient will also be accurate to order ε.

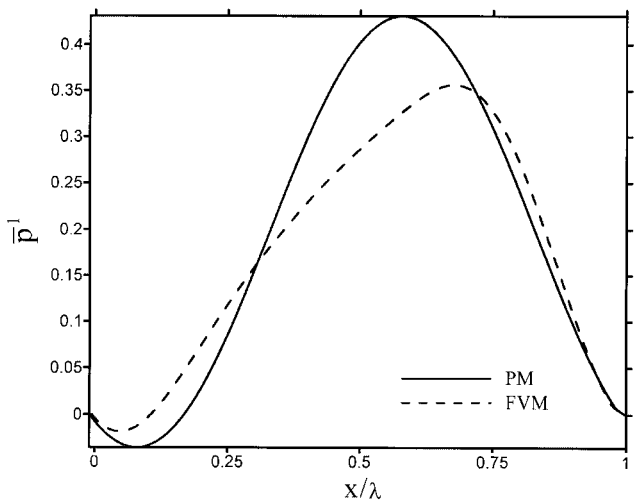

Figure 7. Average fluctuating pressure distribution for $Re = 3000$, $\varepsilon = 0.1$ and $\alpha = 1$. The figure shows the distributions based on the finite-volume and perturbation methods.

The limitations of the proposed perturbation simulation have been quantified based on the error source and validated by comparison from finite-volume simulations. The error on the velocity field increases with ε^2 and is nearly unaffected by α in the range 0.1–100. The error in predicting pressure gradients is of the order of ε. This error is sufficient to cause differences between the finite-volume and perturbation methods of 5% in predictions of macroscopic features such as recirculation bubble lengths. Over the range $Re = 50$–5000, the Reynolds number does not affect the steady-state flow field structure qualitatively, but error in the location of critical points, such as reattachment, does double over this range.

Finally, it is important the issue of CPU and storage requirements is important to address whenever a comparison between two numerical methods is made. For the current study, however, both the perturbation and the finite-volume codes used in the comparison are in-house codes. It should, on the other hand, be clear that the requirements for the perturbation method are practically nil (seconds in CPU for a typical problem), when the code is executed on a modern PC. The finite-volume code requires typically hours in CPU for the same problem.

4. RESULTS AND DISCUSSION

In this section, results are presented in an effort to elucidate some of the intricate physical behaviour that emerges in the flow inside modulated channels. Although some results are already available from the literature, there is yet a need for a systematic investigation of the influence of the various parameters on the flow. In particular, the influence of inertia, modulation amplitude and wavelength will be examined by varying Re, ε and α, respectively.

The influence of inertia is reflected in Figures 8 and 9, which depict the behaviour for $\varepsilon = 0.2$ and $\alpha = 1$, for low-inertia ($Re = 50$) and high-inertia ($Re = 2000$) flows,

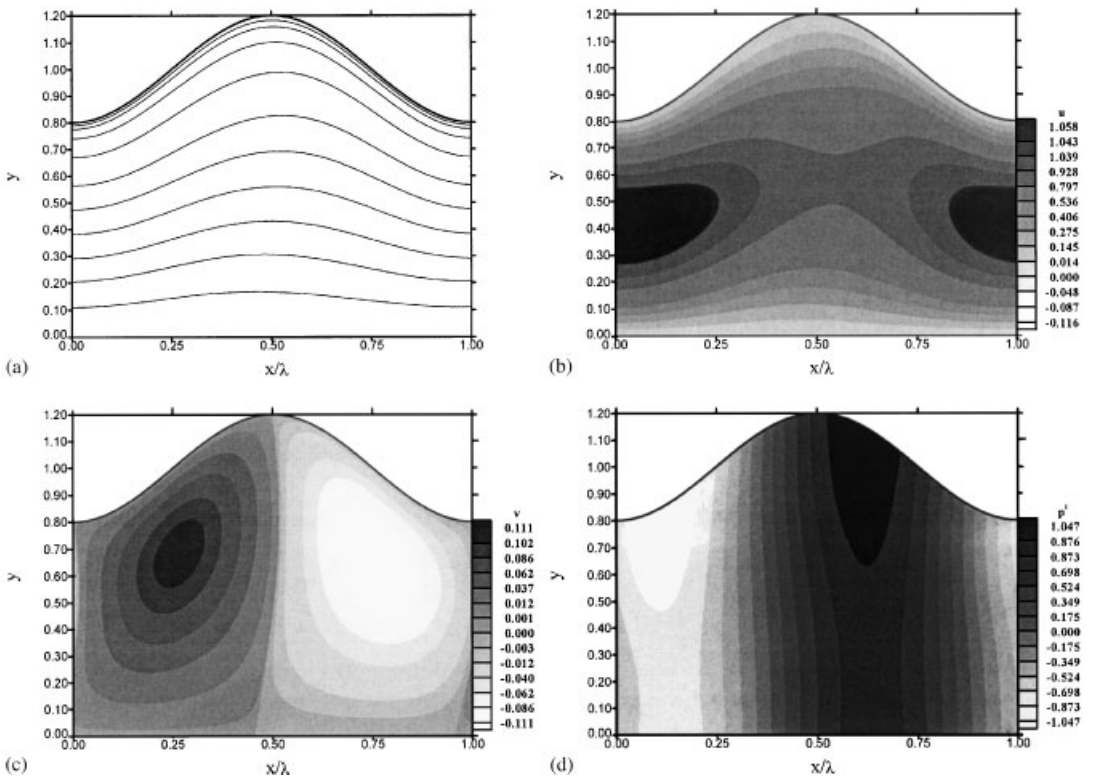

Figure 8. Typical response of a flow at low inertia ($Re = 50$). The figure displays the streamlines (a), the contours of the steamwise (b) and transverse (c) velocity components, and the pressure (d). Here $\varepsilon = 0.2$ and $\alpha = 1$.

respectively. These two cases illustrate the typical behaviours in the pre- and post-critical ranges of Reynolds number. Each figure shows the streamlines, the contours of the velocity components in the streamwise and depthwise directions, and the contours of the pressure deviation, p^1. The same scales are used in both figures for clarity of comparison. The vortex in Figure 9(a) occupies a significant portion of the flow below the crest. There is a loss of symmetry (with respect to $x/\lambda = 0.5$) in the streamlines, which is also reflected in the flow variables, particularly in the u contours. Figures 8(b) and 9(b) indicate that the (dimensionless) maximum streamwise velocity occurs below the trough, which is expected given the relatively strong contraction. The separation causes the velocity to weaken (by about 10% in this case), and the maximum is even more localized below the trough. Other significant topological changes are observed just below the crest because of flow separation. Despite the apparent significance of the backflow, the magnitude of the velocity in the reverse direction is only 10% of the maximum in u. The flow in the depthwise direction in Figure 9(c) also weakens (relative to $U_{\max}$), but remains essentially symmetric as in Figure 8(c). However, the region of maximum v tends to widen because of the separation, indicating a smaller gradient. As to the pressure fluctuation, Figures 8(d) and 9(d) show that p^1 exhibits a minimum below

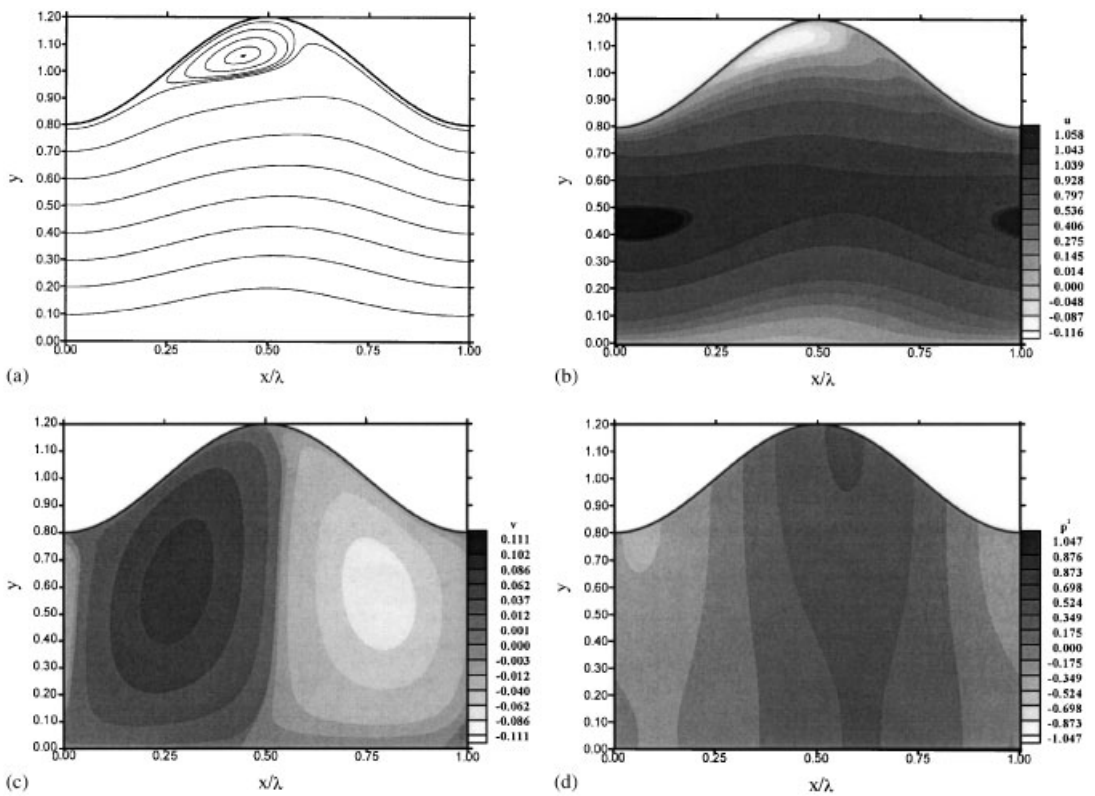

Figure 9. Typical response of a flow at high inertia ($Re = 2000$). The figure displays the streamlines (a), the contours of the streamwise (b) and transverse (c) velocity components, and the pressure (d). Here $\varepsilon = 0.2$ and $\alpha = 1$.

the trough and a maximum below the crest, which are of the same magnitude. The regions of extrema extend further down in the absence of separation. The pressure varies almost linearly with x between the two extrema. As would be expected, the streamwise pressure gradient is much higher for the separated flow case.

The streamwise variation in the shear stress, τ_w, at the modulated wall is shown in Figure 10 for the range $Re \in [500, 3000]$, $\varepsilon = 0.1$ and $\alpha = 1$. The onset of backflow corresponds to τ_w switching sign. In this case, separation occurs at Re slightly below 1500. It is observed that the variation in shear stress is periodic with respect to x, but is out of phase with the variation in wall shape. The amplitude of τ_w increases with Re. Since the flow in two-dimensional and the wall is rigid, the separation and reattachment points are the locations where τ_w is zero. For Re (roughly) below 1500, the shear stress variation is negative, and the flow remains attached. For $Re = 2000$, a separated flow region on the channel wall exists. The value of the Reynolds number for which the flow just separates is often referred to as the critical Reynolds number [11, 12]. Figure 11 displays the influence of inertia on the pressure fluctuation, p_w^1, along the modulated wall, for the same parameters as in Figure 10. It is interesting to observe that the

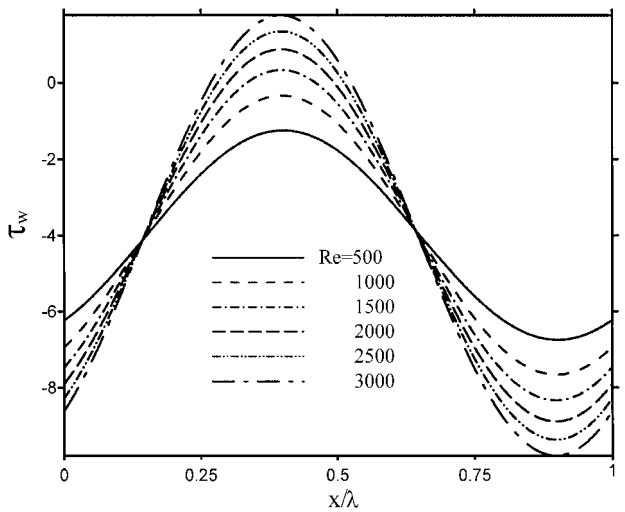

Figure 10. Influence of inertia on the shear-stress distribution at the modulated wall for $\alpha = 1$ and $\varepsilon = 0.1$.

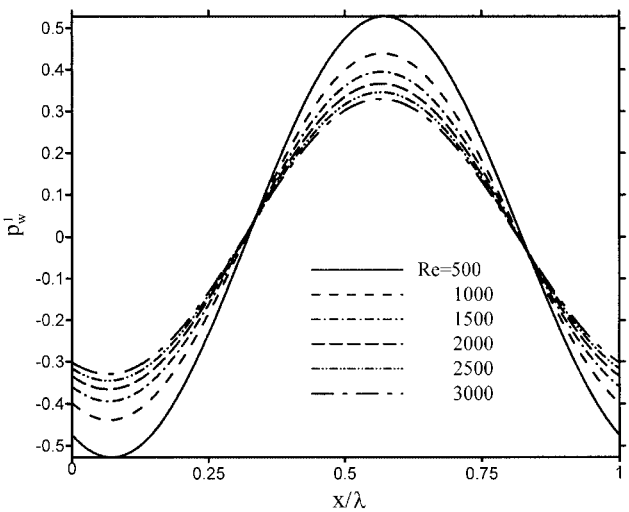

Figure 11. Influence of inertia on the pressure distribution at the modulated wall for $\alpha = 1$ and $\varepsilon = 0.1$.

level of pressure fluctuation decreases as *Re* increases. The results above are in accord with the predictions of Selvarajan *et al.* [11].

The influence of the modulation amplitude, ε, on the location of the points of separation and reattachment as function of the Reynolds number is illustrated in Figure 12 for $\alpha = 1$

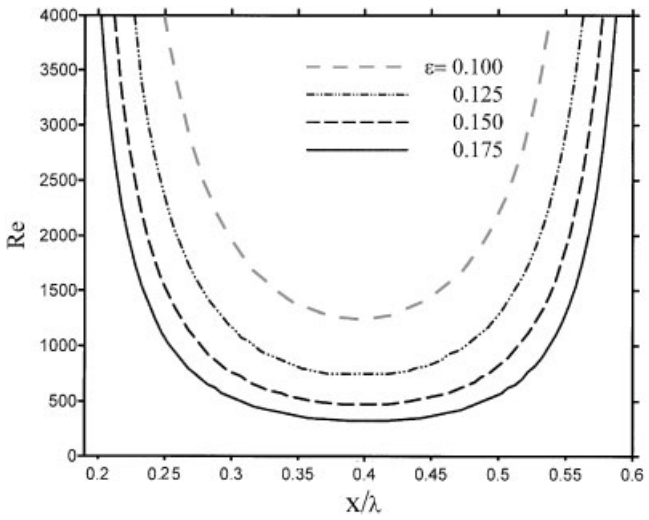

Figure 12. Influence of wall modulation amplitude on the locations of separation and reattachment points against the Reynolds number, for $\varepsilon \in [0.1, 0.175]$ and $\alpha = 1$.

and the range $0.1 \leqslant \varepsilon \leqslant 0.175$. Note that case $\varepsilon = 0$ corresponds to Poiseuille flow, where no separation occurs. At a given Re, the separation point lies to the left, and the reattachment point lies to the right. Typically, for a given ε, a critical Reynolds number, Re_c, is needed for separation to occur. For instance, $Re_c = 1300$ for $\varepsilon = 0.1$. As Re increases above Re_c, the size of the vortex increases until the vortex spans the entire period of the modulation. For small ε, the Re vs x curve is narrow, exhibiting a strong minimum, from which Re_c is readily identified. In contrast, for large ε, the curve tends to flatten, reflecting a weak minimum. Thus, for strong modulation amplitudes, even a slight increase of Re above Re_c leads to the onset of a relatively large vortex. If ε is increased further, a critical value, ε_c, is reached at which separation occurs at a vanishingly small Reynolds number.

The influence of the modulation wavenumber, α, can be significant. The overall influence of the modulation wave number, α, is illustrated in Figure 13, where the positions of the separation and reattachment points are plotted against Re for $\varepsilon = 0.1$. From this figure, it is seen that α has a marked effect on the flow character. Physically, however, the influence of this parameter is less marked than that of ε. For instance, the critical Reynolds number decreases from 1300 to 400 as the length of the modulation is reduced by a factor of two (α increases from 1.0 to 2.2). On the other hand, the critical Reynolds number decreases from 1300 to 400 when ε increases from 0.1 to 0.175, i.e. when the channel maximum-to-minimum width ratio changes by only 6.8% from 1.1 to 1.175.

The value of the critical Reynolds number, Re_c is probably the most important threshold parameter in the problem. Figure 14 shows the variation of Re_c with the wall amplitude, ε, for various values of $\alpha \in [0.6, 2.2]$. Further analysis of the simulation results shows that, for sinusoidal wall modulations, an explicit universal and functional relationship between Re_c, ε

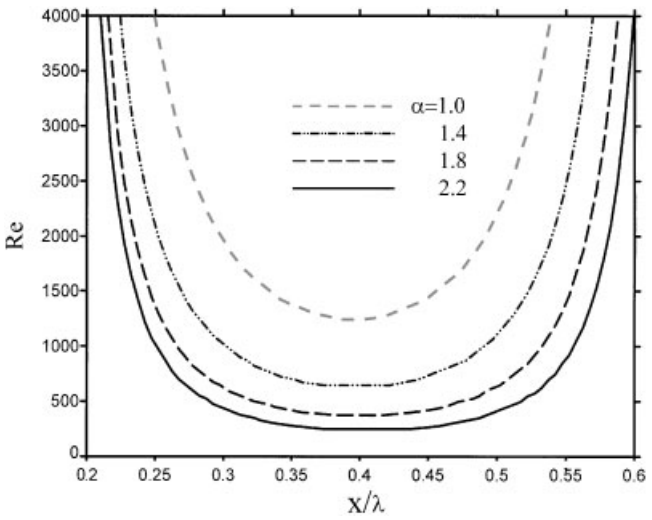

Figure 13. Influence of wall modulation wavenumber on the locations of separation and reattachment points against the Reynolds number, for $\alpha \in [1, 2.2]$ and $\varepsilon = 0.1$.

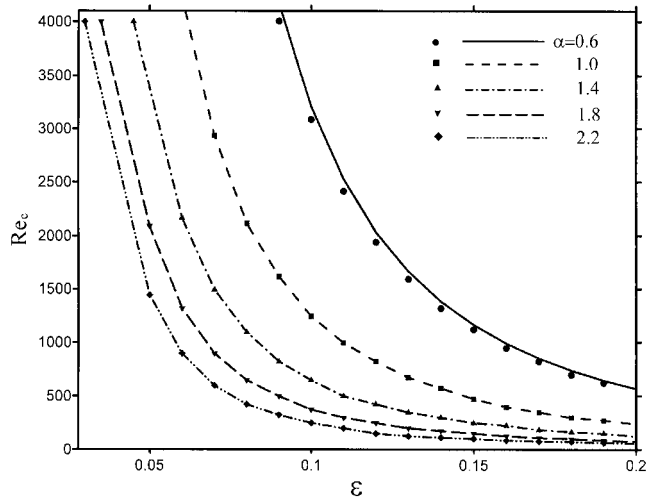

Figure 14. Influence of the wall modulation wavenumber on the critical Reynolds number, Re_c, against the modulation amplitude, ε, for $\alpha \in [0.6, 2.2]$. Symbols indicate the fit from Equation (19).

and α exists, which is given by

$$Re_c = 3.9\varepsilon^{-2.5}\alpha^{-2} \tag{19}$$

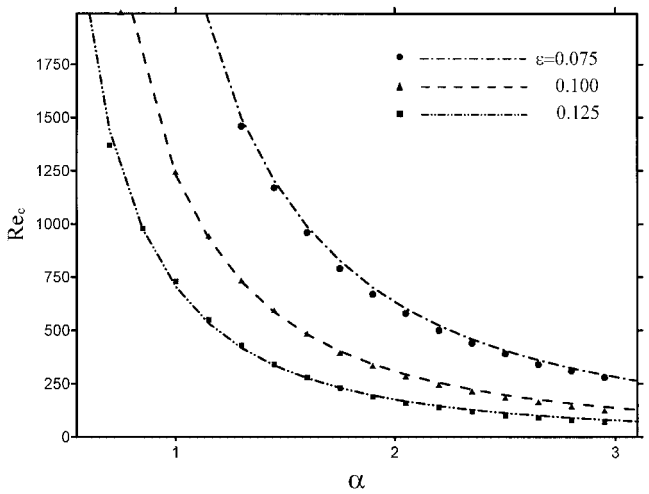

Figure 15. Influence of the wall modulation amplitude on the critical Reynolds number, Re_c, against the modulation wavenumber, α, for $\varepsilon \in [0.075, 0.125]$. Symbols indicate the fit from Equation (19).

The symbols in Figure 14 show the fit of this formula for each curve. The formula shows that the occurrence of separation will depend on the local streamwise pressure gradient and the local wall curvature. Sobey [1] suggested the possible existence of such a relationship. His results indicated a relationship of the type $\varepsilon^{-3}\alpha^{-1}$. However, his parameter domain covered a very small range of α and ε. The relationship of Equation (19) is valid over a larger domain of parameter values. Typically, Re_c decreases dramatically with wall amplitude when ε is small. As ε increases further, the drop in Re_c becomes less pronounced. In fact, there is an asymptotic decrease toward the zero limit. The drop is sharper and convergence (toward zero) is faster as α increases. A similar behaviour is observed when Re_c is plotted against the modulation wave number. The influence of wall wavenumber is inferred from Figure 15.

There is, finally, an additional quantity that is worth examining, namely the average volume (or equivalently mass) flow rate, Q_{ave}, through the modulated channel. It is expected that the flow experiences a loss as a result of wall modulation, under the same driving conditions due to energy losses at the wall. Figure 16 shows the dependence of Q_{ave} on ε. There does not seem to be a particular behaviour that the curve follows. Other parameters, particularly Re and α do not have a significant influence on the volume flow rate. There is, however, a slight loss of volume rate at small α, which is not detected in the figure.

5. CONCLUSIONS

The validity of the perturbation approach for the prediction of flow behaviour inside a channel with weak spatial modulation is assessed in this study. A systematic comparative assessment is carried out against results based on a two-dimensional finite-volume code. The main advantage of the perturbation solution is its ease in implementation, and the low CPU and storage

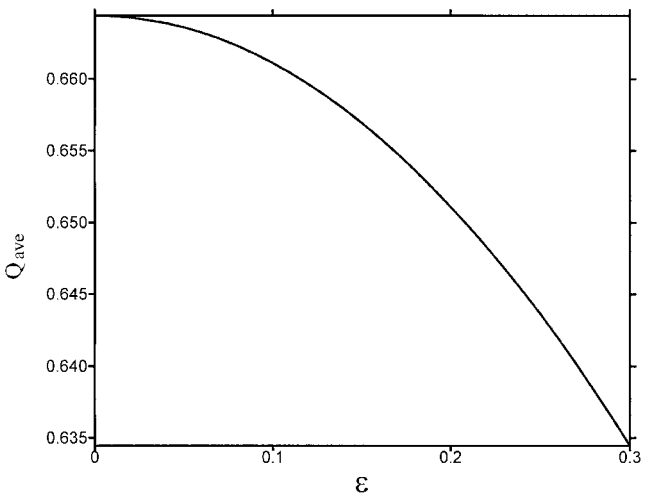

Figure 16. Average volume flow rate plotted against ε. Calculations show that the influence of the modulation wavenumber and inertia is essentially absent. The curve in the figure is essentially universal.

requirement, compared to a full CFD simulation. The influence of inertia, modulation amplitude and wavenumber is particularly emphasized. It is established that the perturbation is globally valid to within the highest-order terms kept in the expansion of velocity and pressure (which, in this case is ε^2). For instance, it is shown that, for $\varepsilon < 0.15$, the two method agree to within 5% for velocity and pressure, and to within 1% for the critical Reynolds number, at which flow separation occurs. Local discrepancies can sometime be higher. The critical Reynolds number is found to follow a universal behaviour as function of wall amplitude and modulation.

ACKNOWLEDGEMENTS

The work is supported by the Natural Sciences and Engineering Council of Canada.

REFERENCES

1. Sobey IJ. On the flow through furrowed channels, Part 1: calculated flow patterns. *Journal of Fluid Mechanics* 1980; **96**:1.
2. Stephanoff KD, Sobey IJ, Bellhouse BJ. On flow through furrowed channels, Part 2: observed flow patterns. *Journal of Fluid Mechanics* 1980; **96**:27.
3. Nishimura T, Ohoriand Y, Kawamura Y. Flow characteristics in a channel with symmetric wavy wall for steady flow. *Journal of Chemical Engineering Japan* 1984; **17**:466.
4. Nishimura T, Murakami S, Arakawa S, Kawamura Y. Flow observations and mass transfer characteristics in symmetrical wavy-walled channels at moderate Reynolds numbers for steady flow. *International Journal of Heat and Mass Transfer* 1990; **33**(5):835.
5. Tanda G, Vittori G. Fluid flow and heat transfer in a two-dimensional wavy channel. *Heat and Mass Transfer* 1996; **31**:411.
6. Sleath JFA. A numerical study of the influence of bottom roughness on mass transport by water waves. *Proceedings of the International Conference on Numerical Methods in Fluid Dynamics*, Southampton, U.K., 1973.

7. Vajravelu K. Fluid flow and heat transfer in horizontal wavy channels. *Acta Mechanica* 1980; **35**:245.
8. Benjamin B. Shearing flow over a wavy boundary. *Journal of Fluid Mechanics* 1959; **6**:161.
9. Dyke MV. *Perturbation Methods in Fluid Mechanics*. Academic Press: New York and London, 1964.
10. Selvarajan S, Tulapurkara EG, Vasanta Ram V. Stability characteristics of wavy walled channel flows. *Physics of Fluids* 1999; **V11**:579.
11. Forrester JH, Young YC. Fluid through a coverging-diverging tube and its implications in occlusive vascular disease, Part I and II. *Journal of Biomechanics* 1970; **3**:297.
12. Selvarajan S, Tulapurkara EG, Vasanta Ram V. A numerical study of flow through wavy-walled channels. *International Journal for Numerical Methods in Fluids* 1998; **26**:519.
13. Wang G, Vanka SP. Convective heat transfer in periodic wavy passages. *International Journal of Heat and Mass Transfer* 1995; **38**:3219–3230.
14. Thompson JF, Warsi ZUA, Wayne Mastin C. *Numerical Grid Generation, Foundations and Applications*. North-Holland: New York, 1985.
15. Caponi EA, Fornberg B, Knight DD, McLean JW, Saffman PG, Yuen HC. Calculations of laminar viscous flow over a moving wavy surface. *Journal of Fluid Mechanics* 1982; **124**:347.
16. Deane AE, Keverkidis IG, Karniakadis GE, Orszag SA. Low-dimensional models for complex flows: application to grooved channels and circular cylinders. *Physics of Fluids A* 1991; **3**:2337.
17. Szumbarski J, Floryan JM. A direct spectral method for determination of flows over corrugated boundaries. *Journal of Computational Physics* 1999; **153**:378.
18. Guzman AM, Amon CH. Flow patterns and forced convective heat transfer in converging-diverging channels. *ASME HTD* 1993; **237**:43.
19. Guzman AM, Amon CH. Transition to chaos in converging–diverging channel flows: Ruelle–Takens–Newhouse scenario. *Physics of Fluids* 1994; **6**:2002.
20. Blancher S, Creff R, Batina J, Andre P. Hydrodynamic stability in periodic geometry. *Finite Elements in Analysis and Design* 1994; **16**:261.
21. El-Soukkary T. Finite-volume model for study of surface-induced motions. *Master's Thesis*, University of Western Ontario, 2000.
22. Mills KD. Flow modifications and instabilities due to periodic corrugation in straight channels. *Master's Thesis*, University of Western Ontario, 2001.

